Journal on Oncology

www.journalononcology.org

Research Article

Open Access, Volume 3

Herbal Medicine Dihydroartemisinin Inhibits Colorectal Cancer by Regulating PI3K/AKT Signaling Pathway

Jia-Ruo Xu[1]; Feng-Jing Jia[2]; Guang-Tao Yao[2]*; Jia-Liang Chen[2]*

[1]Hong Kong Baptist University, Hongkong, China.

[2]Shanghai University of Traditional Chinese Medicine, Shanghai, China.

Abstract

Colorectal cancer (CRC) is the third most prevalent digestive tract cancer worldwide (9.7%), with a severe morbidity and mortality rate. The major therapeutic medications for CRC today are chemotherapy and targeted monoclonal antibodies, however, they all have drawbacks such as high cost, drug resistance, and substantial immunological adverse effects, and not all patients can benefit from them. Dihydroartemisinin (DHA), an artemisinin derivative, has been shown to have antimalarial and anticancer properties against several drug-resistant sensitive cancers. This study examined DHA's anti-cancer properties on RKO cells *in vivo* and *in vitro*. According to an *in vivo* investigation, DHA was more effective at increasing the body weight of tumor-bearing nude mice than cisplatin., 200 mg/kg DHA also significantly reduced tumor weight and volume and lowered blood TNF-α levels, with a tumor inhibitory rate of 41.45%. Network pharmacology and molecular docking approaches were used to examine the inhibitory effect of DHA on CRC cells. The findings suggested that DHA may prevent CRC by controlling the PI3K/AKT signaling pathway. The outcomes of *in vitro* investigations demonstrated that DHA, with an increase in drug concentration and intervention duration, could limit the proliferation and promote apoptosis of RKO cells. Cell cycle arrest occurred in the G2/M phase. After 12 and 24 hours of treatment, 95 µmol/L DHA significantly reduced the ability of cells to migrate and increase the expression of the MMP-9 protein in the cells; It also significantly increased the mRNA expression levels of *Caspase-3*, *Caspase-9*, and the ratio of *Bax*/*Bcl-2*, as well as the levels of cleaved Caspase-9/Caspase-9 and Bax/Bcl-2 protein expression ratio. AKT expression was also markedly decreased by DHA, which also prevented the phosphorylation of p38 MAPK, PI3K, and AKT. In conclusion, DHA can trigger cell apoptosis, reduce tumor growth, and impede the proliferation and migration of CRC RKO cells.

Keywords: Dihydroartemisinin; Colorectal cancer; Cell proliferation and apoptosis; RKO cell; Tumor growth.

Introduction

Colorectal Cancer (CRC), the most common malignant tumor of the digestive tract, has expanded remarkably swiftly in recent years and is linked to high rates of morbidity and mortality as well as ease of recurrence and metastasis [1]. Per the CRC treatment guidelines, surgery and adjuvant chemotherapy are the primary treatment options. Particularly for patients with terminal CRC, surgical therapy for CRC has a risk of recurrence and metastasis, as well as surgical aftereffects including diarrhea or constipation. Cisplatin (DDP) is a potent chemotherapy drug that has a wide anti-cancer spectrum and is not cell-cycle dependent. It is a component of a platinum-based metal complex that inhibits the transcription and replication of intracellular DNA or binds to nuclear proteins and plasma proteins to have an anti-cancer

Manuscript Information: *Received: Feb 03, 2023; Accepted: Mar 16, 2023; Published: Mar 27, 2023*

Correspondance: *Jia-Liang Chen & Guang-Tao Yao, Shanghai University of Traditional Chinese Medicine, Shanghai, China.*

Email: 409786396@qq.com & yaoguangtao1969@126.com

Citation: *Xu JR, Jia FJ, Yao GT, Chen JL. Herbal Medicine Dihydroartemisinin Inhibits Colorectal Cancer by Regulating PI3K/AKT Signaling Pathway. J Oncology. 2023; 3(1): 1080.*

action [2,3]. However, its widespread use is restricted due to its toxicity to healthy cells and other harmful side effects. Therefore, the development of anti-tumor medicines with novel modes of action and low toxicity has garnered interest to suppress the development of CRC and prevent tumor spread and recurrence.

Traditional Chinese medicine is a cultural gem of China. More academics are focusing on the clinical research of natural medicine in the area of cancer because of the benefits of TCM treatment based on syndrome distinction, treatment of non-diseases, and multi-target therapy. The mechanism of action of TCM is unclear due to its complex chemical components, multiple targets, and multi-level pharmacological effects. However, a novel tool and approach for determining the mechanism of therapeutic action are provided, which stimulates the modernization and globalization of TCM. It combines the target database of TCM in many diseases with molecular docking verification and network pharmacology. The development and application of systems biology, which includes contemporary genomics, proteomics, and metabolomics, is where the idea of network pharmacology originated. To support and offer a significant amount of data on the interaction of biological entities, large-scale biological databases are required. The traditional search for a single target in pharmacological research will give way to thorough network analysis, such as through the creation of a «target drug-disease-gene» network. A new tool and concept for analyzing the mechanism of drug action were developed by analyzing and observing the influence of drugs on diseases [4,5]. This method is similar to «treating the same disease with different diseases» and «treating the same disease with the same disease» in traditional Chinese medicine theory.

Artemisia annua was included as a remedy for malaria in Ge Hong's «handbook of medicines for emergencies» during the Eastern Jin Dynasty: «Artemisia annua a grip, with two liters of water stains, wring juice, to drink it.» Artemisinin is the most effective medication for treating malaria resistance. *Artemisinins* and their derivatives display powerful anticancer potential in addition to their anti-malarial properties, according to more recent studies [6]. DHA is one of the most studied derivatives used to treat malignancies. Studies have demonstrated that DHA has inhibitory effects on the proliferation and growth of a range of tumor cells, including cervical cancer cells, lung cancer cells, oesophageal squamous carcinoma cells, gastric cancer cells, and liver cancer cells [7-11], supporting the idea that DHA is a potentially effective anti-tumor agent. However, few *in vivo* research on DHA in the therapy of CRC have been described, and the majority of these are *in vitro*.

In this study, the inhibitory impact of DHA on subcutaneously transplanted tumors in nude mice was assessed. The inhibitory impact of DHA on CRC cells and its probable mechanism were then evaluated using network pharmacology and molecular docking approaches. Using the RKO cell line, we checked into whether DHA may trigger endogenous apoptosis and block the cell cycle in the G2/M phase by inhibiting the PI3K/AKT signaling pathway. These results will serve as an experimental foundation for the application of DHA in the therapy of CRC.

Materials and methods

Drugs and reagents

DHA was synthesized and gifted by the group of Zhang Wanbin of Shanghai Jiaotong University with a purity of >99%. 25 mg of Cisplatin/stem (Sigma-Aldrich, USA). A 0.2 mg/ml solution was mixed with ordinary saline before use. The solution was ultrasonically solubilized and stored at 4°C.

Animals

Sixty male nude rats of SPF grade, 6-7 weeks old, weighing 24 ± 2 g, were purchased from Shanghai Siple-Bikai Laboratory Animal Co.

All experimental protocols involved were approved by the ethics committee of the Shanghai University of Traditional Chinese Medicine (PZSHOTCM201113011). The experimental animals were kept under standard housing conditions, with a temperature of 20-25°C, Relative humidity was maintained between 40% and 60%, and normal day and night cycles.

Tumor xenograft model

RKO human colorectal cancer cells were altered to 1×10^7 cells/ml. To establish a subcutaneous xenograft tumor model in nude mice, the mixed cells were resuspended and injected subcutaneously into the left axilla of the animals using 0.2 ml of cell suspension. In nude mice, the development of xenograft tumors was observed and recorded. Mice were randomly allocated to one of four groups after model building. Drug delivery was begun after the tumor's diameter reached about 5 mm.

Three times per week, a 2 mg/kg intraperitoneal injection of cisplatin was given to the Cisplatin group. The DHA groups received either a high dose (200 mg/kg/d) or a low dose (100 mg/kg/d) of DHA. The model group received 10 ml/kg/d of normal saline. The medication was given constantly for 30 days. Daily observations of mice's activity, mental state, skin, and diet were made by modeling. The medication was given when the transplanted tumor's diameter tumor was more than 5 mm. The major diameter (L) and transverse diameter (W) of the transplanted tumor were measured and recorded with electronic vernier calipers. The tumor volume was calculated using the formula: tumor volume (V,mm3)=[l(mm) X W2(mm2)]/2. The tumors' growth curve was depicted. the pharmacological intervention was terminated on the 31st day, and the blood was collected from the intraocular venous plexus of the mice. The mice were sacrificed. The mice's subcutaneous transplanted tumors underwent exfoliation and weighing. Utilizing the formula, the tumor inhibition rates of different groups were obtained:

tumor inhibition rate (%) = (1 − Treatment Group average tumor weight ／ Model Group average tumor weight) ×100%.

Hematoxylin-eosin staining (H&E)

The exfoliated tumors were stored at 4°C after being fixed in a 4% paraformaldehyde solution. The microtome rack held the prepared tumor paraffin slices, which were then moved to the staining box. The staining steps are as follows: xylene, 10 min twice; absolute ethanol, 5 min twice; 95% ethanol, 5 min; 90% ethyl alcohol, 5 min; 80% ethanol, 5 min; 70% ethanol, 5 min;

Washed repeatedly with distilled water and drain. The sections were stained with hematoxylin for 3-8 min and then washed under running water. Differentiation with 1% HCL for a brief period of time, followed by a rinse under running water; 0.6% ammonia water converted the rinse back to blue. Eosin dye was used to stain the sections for 1-3 min, after which 95% ethanol was added successively for 5 min, twice. Absolute ethanol, twice for 5 min each, as well as xylene. Following drying, the portions were dehydrated and coated with neutral gum. Images were gathered for examination after being examined under a microscope.

Enzyme-linked immunosorbent assay for TNF-α levels

Before the execution of each group of mice, blood was drawn from the posterior ocular plexus into 1.5 ml EP tubes in an amount of about 0.5 ml. Each tube containing a sample of whole blood had its information marked. They were kept there overnight at 4°C. The blood was centrifuged at 1000 rpm for 15 minutes to prevent repeated freezing and thawing. The supernatant was then separated into new EP containers and kept at -80°C. Thawed samples should be centrifuged before testing them. According to the instructions on the kit, serum samples from each group should be taken to evaluate the TNF-α (NeoBioscience, China).

Target prediction of DHA and network construction

The CAS number of DHA (71939-50-9) was input into the PubChem [12] (https:// pubchem.ncbi.nlm.nih.gov) for retrieval of DHA, and the SMILES number [CC1CCC2C(C(OC3C24C1CCC(O3)(OO4)C)O)C] and structural data were saved. SMILES number of DHA was input into SWISS [13] (http://www.swisstargetprediction.ch/index.php), «Homo sapiens» was selected to limit the source of screened species, and target prediction was carried out based on structural similarity. The target in prediction results was selected and set as DHA target file.csv. Select «Ingredient» in SymMap [14] (https://www.symmap.org/) and enter « dihydroartemisinin» to retrieve. Then the targets obtained from the two databases were summarized and de-processed to integrate a comprehensive drug target database. «Colon cancer» was entered into GeneCards [15] (https://www. genecards.org) for retrieval, and the obtained disease gene target score was sorted in descending order.

The obtained DHA predicted target genes and colon cancer gene targets were respectively input into the corresponding positions in the Draw Venn Diagram (http://bioinformatics.psb.ugent.be/webtools/Venn/), and the gene intersection was compared, and the Venn diagram was drawn, and the common cross-target genes were extracted as potential targets of DHA in the treatment of CRC.

In order to collect the PPI Network data, the common target genes following the intersection were submitted to String (https://string-db.org/cgi/input.pl) [16]. The PPI network data was then used to construct the drug-disease target protein interaction network using Cytoscape software. The Network Analyzer function of the Degree value was used to evaluate the PPI network and modify the size and color of each target node in the PPI network (connection degree).

Molecular docking analysis

Prepare protein Using the «Prepare Protein» function in the Discovery Studio 4.0 software, the active sites were defined after the protein was dehydrated, hydrogenated, repaired the defect area, and optimized the structure. Since the protein crystal structure used for molecular docking this time, all contain small molecule inhibitors, the binding site of each small molecule inhibitor is directly defined as the active site, and the radius of the active site is set to 5-10 A according to different situations of each protein.

Small molecule preparation Using the «prepare ligands» function in the software, the small molecule was optimized, and conformation search was conducted, and only one conformation was obtained when the DHA molecule was prepared. To prepare for molecular docking, the conformation with the minimum energy was determined after «full minimization» had optimized the conformation's energy. The software's «CDOCKER» function was used to perform molecular docking, with RMSD defined to 0.5 and the other parameters left to their default values.

Enrichment analysis

To undertake the GO biological process and KEGG pathway enrichment analysis of the potential target of DHA in the CRC treatment, the common target genes were imported into the David [17] (https://david.ncifcrf.gov) database, and the species «Homo sapiens» was chosen. GO is a biological functional system, which is used to define the function and features of gene products. For the GO analysis, three modules - biological process (BP), cell composition (CC), and Molecular Function (MF) - were chosen. The pathway analysis method of choice was the KEGG module. KEGG pathway enrichment analysis was created to obtain much richer biological pathways, more efficiently connect link gene lists with higher-order functional information, and systematically examine gene function. By screening the FDR less than 0.05 GO biological process and KEGG enrichment data (P<0.05), the top 20 signaling pathways were identified. The amount of genes (count value) enriched in each pathway were ranked in descending order. Bioinformatics (http://www.bioinformatics.com.cn/) then displayed the analysis results.

Cell culture

Human colon cancer RKO cells, purchased from the Cell Resource Center of Shanghai Institutes for Biological Sciences, Chinese Academy of Sciences. The RKO cell line was cultured in RPMI 1640 medium containing 10% fetal bovine serum and 1% penicillin-streptomycin test solution which was placed in a 37°C, 5%_CO_2 cell culture incubator. The cells were changed every 1-2 d according to their growth status and passaged once every 2-3 d.

Cell proliferation assay

RKO cells were planted in 96-well plates at a density of 1 × 10^4 cells/ml and 100 µl per well during the logarithmic growth phase. Based on the concentration of DHA interventions were administered (0, 25, 50, and 100 µmol/L) (the solution had a volume of 100 µl, and the 0 µmol/L groups were given a medium containing equal levels of DMSO). Each well received 20 µl MTT reagent (5 mg/ml, (Sigma-Aldrich, USA)) after 12, 24, 48, and 72 h of incubation. Incubation was then continued for 4 h. Carefully removing the culture medium, 150 µl of DMSO was applied to

each well. After shaking in the dark for 10 min, the absorbance (OD) was evaluated at 570 nm in a microplate reader. The inhibition ratio of cell proliferation was calculated.

Cell apoptosis detection by flow cytometry

At the point of logarithmic growth RKO cells were collected. After optimizing the cell density to 2.5 × 10^5 cells/ml and inoculating the cells at 2 ml/well onto 6-well plates (confocal dishes), the medium was removed once the cells had become adherent. Different concentrations (0, 50, 95, 150 µmol/L) of DHA were given and cells were collected for subsequent detection after 48 h of incubation. After 48 h of cell grouping and drug intervention, cells were harvested and washed twice with pre-cooled DPBS. The cells were resuspended by adding 150 µl of 1×Binding Buffer to the cell precipitate to make the cell density reach 1 × 10^6 cells /ml. A fresh centrifuge tube was filled with 100 µl of cell suspension, and then 5 l Annexin V-FITC and 10 µl PI reagent (Meilunbio, China) were gently added, combined, and incubated for 15 min at room temperature in the dark. Flow cytometry was used to assess cell apoptosis.

Hoechst 33258 staining for detection of cell apoptosis

After 48 h of cell grouping and pharmacological intervention following «2.11», the growth medium was aspirated, 0.5 ml of fixation solution was applied, and the cells were fixed overnight at 4°C. The next day, the fixative was discarded after being cleaned twice for 3 min each with DPBS. 0.5 ml of Hoechst 33258 staining solution (Meilunbio, China) was applied to stain for 5 min. Then, it was rinsed twice for 3 min each with 0.5 ml of DPBS. The liquid was aspirated. The anti-fluorescence quenching solution was included. A fluorescence microscope was used to capture images of the cell apoptosis.

Cell cycle assay

After 48 h of cell grouping and medication intervention following «2.11», cells were harvested. The mixture was centrifuged at 1,000 rpm for 5 min after adding 1 ml of pre-cooled DPBS. The supernatant was removed. 1 ml of DPBS was given and resuspended. 3 ml of pre-cooled anhydrous ethanol was gradually added dropwise until the ethanol concentration reached 75%, and stored overnight at 4°C.

According to the kit's instructions, the staining solution (staining buffer: PI staining solution: 50×RNase A=100:5:2) (Meilunbio, China) was prepared in advance and kept at 4℃ for later use. After removing the fixed cell suspension and centrifuging the supernatant, the cells were resuspended by adding 1 ml of chilled DPBS.

Each tube of the sample received 500 µl of pre-prepared staining working solution, and then the cells were gently mixed before being incubated for 30 min at 37℃ in the dark. The supernatant was then absorbed and discarded. The cell cycle was determined by flow cytometry.

Wound healing assay

RKO cells were adjusted density to 5 × 10^6 cells /ml and then planted in 6-well plates. A 200 µl micropipette was used to create three parallel wounds perpendicularly to the plate plane after the cells had become adherent and overgrown. To get rid of the cell debris, DPBS was applied three times to the cells. DHA was supplied at 0 and 95 µmol/L amounts, respectively. under a microscope, the wounds were captured at 0, 6, 12, and 24 h. The area of the blank area was measured by using ImageJ software and the cell migration rate was calculated.

Real-time quantitative PCR assay

RKO cells at the logarithmic growth stage were obtained, and the cell density was regulated to 3 × 10^5 cells/ml. 2 ml/well cells were then seeded in 6-well plates. DHA at concentrations of 0 and 95 µmol/L was added, respectively. After 12 h of cell grouping and drug intervention, cells in each group were collected, and total RNA was extracted by adding 1 ml TRIzol reagent and 200 µl chloroform. Then reverse transcription reaction was carried out according to the kit (CWBio, China) instructions to prepare cDNA. The mRNA expression levels of *Caspase-3*, *Caspase-9*, *Bcl-2*, and *Bax* in each group were detected by fluorescence quantitative PCR with *β-actin* as the internal reference. All the primers were synthesized by Shanghai Shenggong Bioengineering Co., LTD. The sequence of primers is shown in Table 1.

PCR reaction conditions: 95℃ for 30 s; 45 cycles of 95℃ for 5 s and 60℃ for 30 s. Dissolution curve analysis: 95℃, 15 s; 60℃, 1 min; 95℃, 15 s; 50℃ for 30 s. The relative mRNA expression level was quantitatively analyzed by the $2^{-\Delta\Delta CT}$ method.

Table 1: Primer sequences of target genes.

Primer name	Specific sequence
Caspase-3	Forward: 5'-CCAAAGATCATACATGGAAGCG-3'
	Reverse: 5'-CTGAATGTTTCCCTGAGGTTTG-3'
Caspase-9	Forward: 5'-GACCAGAGATTCGCAAACCAGAGG-3'
	Reverse: 5'-AAGAGCACCGACATCACCAAATCC-3'
Bax	Forward: 5'-CGAACTGGACAGTAACATGGAG-3'
	Reverse: 5'-CAGTTTGCTGGCAAAGTAGAAA-3'
Bcl-2	Forward: 5'-CATGCTGGGGCCGTACAG-3'
	Reverse: 5'-GAACCGGCACCTGCACAC-3'
β-actin	Forward: 5'-GGGACCTGACTGACTACCTC-3'
	Reverse: 5'-TCATACTCCTGCTTGCTGAT-3'

Western blot

Inoculating cells onto 60 mm culture dishes after adjusting the cell density to 1 × 10^7 cells/ml. DHA was added in various concentrations: 0, 50, and 95 µmol/L. After 48 h of drug intervention, 200 µl of mixed lysis solution (RIPA lysis solution with protease and phosphatase inhibitor) was added, and it was then lysed on ice for 30 min. The total protein concentration of cells was calculated using the BCA method. polyacrylamide gel electrophoresis (70 V, 50 min; 120 V, 1 h) was applied to separate each well which contained 40 µg of protein. Transferring the isolated proteins to PVDF membranes (0.2 A, 2 h).

5% skim milk was added and blocked on a table concentrator for 2 h at room temperature. The membrane was cleaned three times with TBST for 10 min each time; primary antibodies to each target protein were added (1:1,000 volume dilution) and incubated overnight at 4°C, antibodies to MMP-9 (Batch No. 13667), Caspase-3 (Batch No. 14220), caspase-9 (Batch No. 9508), clea-

ved Caspase-3 (Batch No. 9661), cleaved Caspase-9 (Batch No. 7237), Bcl-2 (Batch No. 5023), Bax (Batch No. 4223), PI3K (Batch No. 4257), AKT (Batch No. 4691), p-PI3K (Batch No. 4228), p-AKT (Batch No. 4060) and, p38 MAPK (Batch No. 8690), p-P38 MAPK (Batch No. 4511), and β-actin (Batch No. 3700) all from Cell Signaling were used. The membranes were washed 3 times with TBST for 10 min each time. Then, primary antibodies were added (1:1,000 v/v) and reacted overnight at 4°C. The membrane was cleaned with TBST 3 times the following day for 10 min each time. Horseradish peroxidase-labeled secondary antibody (volume dilution ratio of 1:5000) was then given and processed for 2 h at room temperature on a table concentrator. The membrane was then given 3 TBST washes, each lasting 10 min. Exposure development was performed with a gel imaging system following the ECL kit's instructions. By utilizing the ImageJ image analysis management system, the protein bands were quantified.

Statistical analysis

SPSS 16.0 software was used for statistical data analysis, and GraphPad 9.0 software was used for plotting. The measurement data were expressed as x±SD. The one-way ANOVA was used for comparison between multiple groups. A T-test was used for multiple comparisons. The difference was considered statistically significant at $p<0.05$.

Results

Effects of DHA on the growth of RKO tumor-bearing nude mice

A subcutaneous tumor developed about 9 days after RKO cells were injected, and the transplanted tumor had a diameter of 5 mm. In comparison to the model group, the mice receiving cisplatin were depressed, sluggish to react, and consumed less food after delivery. Both the high- and low-dose DHA groups of mice displayed improved mental health, increased activity, and normal eating habits. Mice in the cisplatin group demonstrated a significant loss of body mass when compared to the model group after 30 days of the administration ($P<0.01$), while mice in the low-dose group showed an increase in body weight ($P<0.05$); Mice in the high and low dose DHA groups displayed a considerable increase in body mass, in contrast to mice in the cisplatin group ($P<0.001$) (Table 2). These results indicated that, in contrast to cisplatin, DHA could greatly improve the tumor-bearing mice's growth status.

Table 2: Effects of DHA on body weight in RKO tumor-bearing nude mice.

Group	Body Weight (g)	
	Before treatment	After treatment
Model	23.67 ± 1.32	30.08 ± 1.52
Cisplatin	23.63 ± 1.05	26.61 ± 1.55**
DHA Low Dose	24.82 ± 0.69	32.08 ± 1.33*###
DHA High Dose	24.81 ± 1.18	31.17 ± 2.17###

(n=10, data represent mean ± SD; **$P<0.01$, *$P<0.05$ vs Model; ###$P<0.001$ vs Cisplatin).

Effects of DHA on the growth of RKO transplanted tumors

The treatment was started when the mice had subcutaneous transplanted tumors more than 5 mm in diameter. The tumor volume in each group was measured by vernier calipers every 4 days, and the growth curve of the RKO tumor was displayed in Figure 1 (A) and (B). The mice were sacrificed on day 31 and the weight of the exfoliated tumor tissue was recorded. As indicated in Figure 1 (C), the tumor inhibition rate was evaluated. After administration, the high-dose DHA group and the cisplatin group significantly inhibited tumor volume as compared to the model group. The cisplatin group showed the highest rate of tumor inhibition (60.80%), followed by the 200 mg/kg DHA group (41.45%), while the 100 mg/kg DHA group had no inhibitory impact on the RKO implanted tumor.

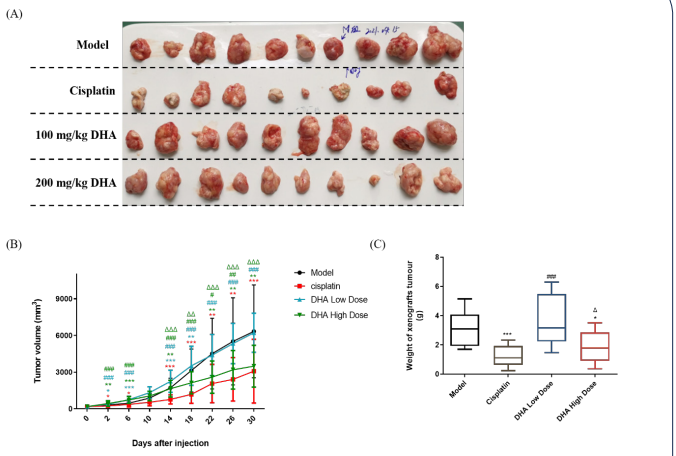

Figure 1: Effects of DHA on the growth of RKO transplanted tumors. **(A)** The growth of subcutaneously transplanted tumors in each group. **(B)** Effect of 30 days of administration on subcutaneous graft tumor volume in each group (n=10, data represent mean ± SD; ***P<0.001, **P<0.01, *P<0.05 vs Model; #P<0.05, ##P<0.01, ###P<0.001 vs Cisplatin; ΔΔP<0.01, ΔΔΔP<0.001 vs DHA Low dose). **(C)** After 30 days of treatment, the weight of the RKO transplanted tumor in each group was measured (n=10, data represent mean ± SD; ***P<0.001, *P<0.05 vs Model; ###P<0.001 vs Cisplatin; ΔP<0.05 vs DHA Low dose).

Pathomorphological changes in tumors

To further clarify the inhibitory effect of DHA on tumors, H&E staining was used for the pathological analysis of tumor cells. H&E staining results revealed that tumor cells in the model group grew in like nests with low differentiation and a large number of nuclear divisions could be observed, as seen in Figure 2 (A). Tumor cells in the cisplatin group grew in a nested pattern and necrosis was visible in the tumor cell foci, which were smaller than those in the model group, as shown in Figure 2 (B).

As shown in Figure 2 (C), the tumor cells in the low-dose DHA group exhibited nest-like proliferation and nuclear division, as well as little differentiation and necrosis. In the high-dose group, the tumor cells developed in a nested pattern, and the cell foci underwent a great deal of necrotic apoptosis, as seen in Figure 2 (D).

As evident from the results of H&E staining, indicating that DHA impeded human CRC cancer cell growth, and induced apoptosis in vivo. It provided a way for in vitro research on the mechanism.

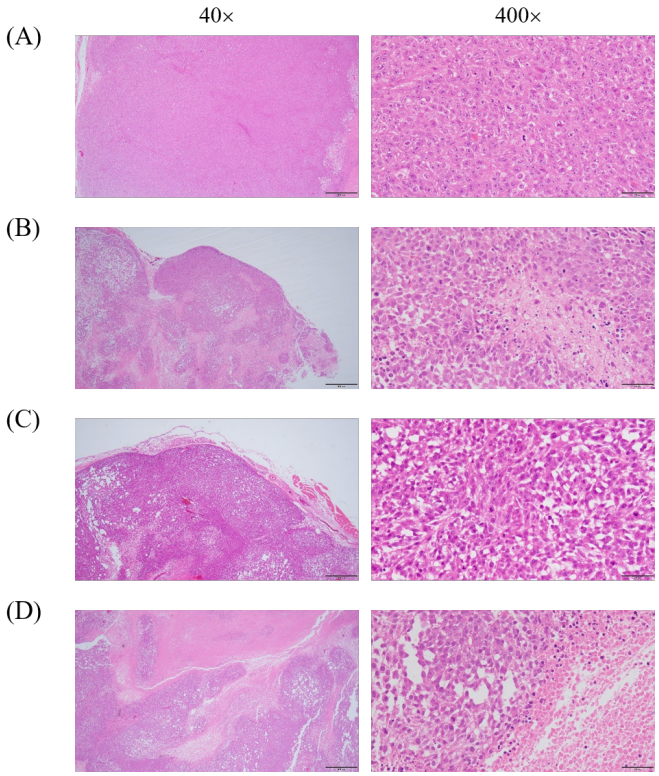

Figure 2: Pathomorphological changes in tumors. **(A)** Model; **(B)** Cisplatin; **(C)** DHA Low Dose; **(D)** DHA High Dose.

Effects of DHA on tumor TNF-α levels

Elisa was used to measure the amount of TNF-α in each group of mice's peripheral blood. The results demonstrated that there was no statistically significant difference between the cisplatin group and the model group in serum TNF-α levels (P>0.05). The content of TNF-α exhibited a statistically significant reduction in both the high and low DHA dosage groups (P<0.05, P<0.01). Figure 3 demonstrated that when compared to the cisplatin group, the inhibitory effect on TNF-α level was more substantial (P<0.05).

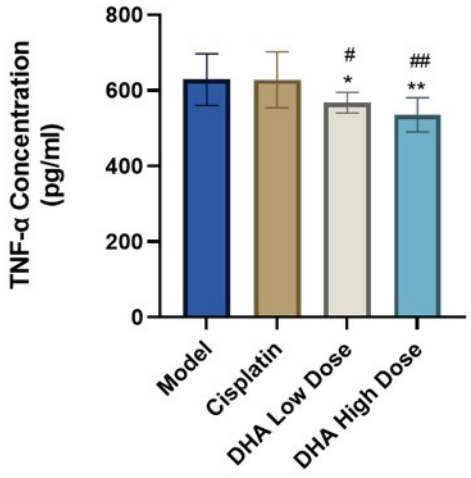

Figure 3: TNF-α levels of each group in serum were detected by Elisa kit. (n=8, data represent mean ± SD; **P<0.01, *P<0.05 vs Model; ##P<0.01, #P<0.05 vs Cisplatin).

Targets identification and PPI network establishment

A total of 98 targets of DHA were obtained by SWISS and SymMap. GeneCards retrieval yielded a total of 21264 CRC-related targets, and the top 1088 targets were chosen by the score in descending order. Drawing a Venn Diagram database allowed for the matching analysis of the target of DHA and genes related to CRC, and 34 overlap targets were chosen, as shown in Figure 4 (A), to indicate the target of DHA for the treatment of CRC.

The 34 intersection targets of DHA-CRC were imported into the String to obtain the protein interaction data (Figure 4 (B)), and then imported into Cytoscape to optimize the construction and analysis of the PPI network (Figure 4 (C)). The PPI network had an average node degree of 10.82, 34 nodes (common target genes), and 368 edges. And the targets of the DHA's anti-CRC effect were represented by the nodes in the diagram. In Figure 4 (C), the correlation is better, the nodes are larger, the color is darker, the degree is higher, and the overall score value is greater. Following Cytoscape Network analysis, the degree value for each target was determined, and the top 5 degrees were EGFR, MAPK1, MAPK3, ERBB2, and PIK3CA.

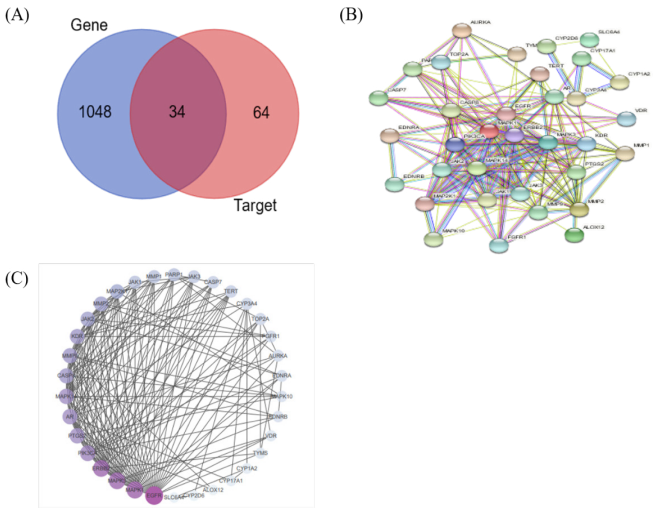

Figure 4: Potential target genes and PPI network map of DHA treatment for CRC. **(A)** Venn diagram of the intersection of DHA targets and CRC genes. **(B)** Potential target interaction of DHA in the treatment of CRC. **(C)** DHA in the treatment of CRC PPI Network.

Molecular docking

For the purpose of molecular docking verification, DHA was utilized as a ligand and the top 5 proteins in the PPI network-EGFR, MAPK1, MAPK3, ERBB2, and PIK3CA-were used as receptors. As shown in Figure 5, all 5 proteins can bind to small molecules. The sequence of force strength was as follows: MAPK3>MAPK1>ERBB2>EGFR >PIK3CA. According to the CDOCKER INTERACTION ENERGY score, the molecule had a moderate intensity interaction with the five proteins, ranging from 24 to 32.

TYR53, VAL56, ALA69, LYS71, LEU173, and CYS183 of the MAPK3 protein all interacted with small molecules on an alkyl-alkyl basis. The small molecules could be effectively mixed in the pocket and interacted with more amino acid residues despite the weak contact force itself (Figure 5 (D)).

MAPK1's ILE31, VAL39, ALA52, LEU107, ASP111, LEU156, and

CYS166 interacted with GLY32 via weakening hydrogen bonds and alkyl-alkyl interactions with small molecules. Despite having larger contact forces, the MAPK1 protein's function was less powerful than the MAPK3 protein because of its greater distance (Figure 5 (C)).

The ERBB2 protein interacts with small molecules via four alkyl-alkyl interactions at LEU726, VAL734, and CYS806. It was evident that there weren't many forces acting, which made the binding weak (Figure 5 (E)).

The EGFR protein's VAL726, LSY745, and LEU844 interacted with one another in a weak alkyl-alkyl-alkyl manner. It had weak hydrogen bonding with ASP855 and strong hydrogen bonding with LYS745, ARG841, ASN842, and THR854. The interaction was weak despite the high force because the vast cavity of the protein prevented small molecules of this shape from being bound to the active site, despite the force being substantial (Figure 5 (B)).

The PIK3CA protein displayed mild alkyl interactions with MET772, ILE848, and ILE932. Additionally, the PIK3CA protein's SER774 and SER919 exhibited hydrogen bonds with small molecules, resulting in a weak overall interaction, which caused them to be ranked last (Figure 5 (F)).

In conclusion, the top 5 primary targets that were strongly related to DHA in the treatment of CRC were identified by Cytoscape's analysis of PPI Network data, and molecular docking was carried out to foretell the interaction between receptor and ligand. These were the sequencing results: MAPK3>MAPK1>ERBB2>EGFR>PIK3CA, indicating that DHA may primarily regulate MAPK3, MAPK1, ERBB2, EGFR, and PIK3CA to prevent CRC.

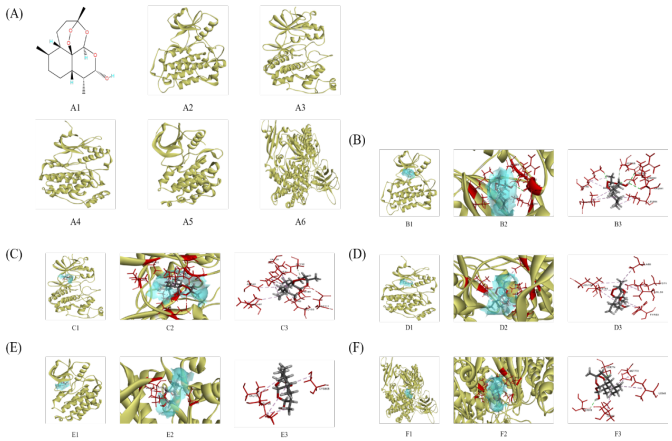

Figure 5: The molecular docking between the hub targets and DHA. **(A)** A1 is the molecular structure of DHA, and A2, A3, A4, A5 and A6 are the protein structure of EGFR, MAPK1, MAPK3, ERBB2 and PIK3CA, respectively. **(B)** Diagram of docking DHA with EGFR protein. **(C)** Diagram of docking of DHA with MAPK1 protein. (D) Diagram of docking of DHA with MAPK3 protein. **(E)** Diagram of docking of DHA with ERBB2 protein. **(F)** Diagram of docking of DHA with PIK3CA protein.

GO biological processes and KEGG enrichment pathway analysis

The GO function was applied to the target gene to clarify the biological characteristics of the target. Figure 6 (A) displayed 15 BP enrichment analyses (including energy pathway and signal transduction), while 9 CC and 12 MF enrichment analyses were selected based on the count value. For specific items, see Table S1. The results of the GO biological process analysis suggested that DHA might inhibit CRC by influencing a variety of biological processes, including protein, protease, enzyme, heme, and iron binding in the cell membrane, cytoplasm, mitochondria, receptor complex, cytoskeleton, and extracellular matrix.

A KEGG pathway enrichment analysis was carried out to investigate the potential mechanism of action of DHA in the therapy of CRC. The results revealed that 34 target genes were assigned to 86 KEGG pathways, and the top 20 pathways were then further evaluated by the count value, as shown in Table S2. The analysis results were then visualized by the micro message platform (Figure 6 (B)). The tumor signaling pathway had the highest number of target connections (count=17), and proteoglycan had 11 targets in cancer, followed by the PI3K/AKT signaling pathway with 10 targets. PI3K/AKT involves multiple targets such as EGFR, MAPK1, MAPK3, and PIK3CA, which were strongly linked to the growth, differentiation, apoptosis, migration, and adhesion of tumor cells. Based on these results, it was theoretically conceivable to treat CRC by utilizing DHA to prevent the PI3K/AKT signaling pathway from becoming activated.

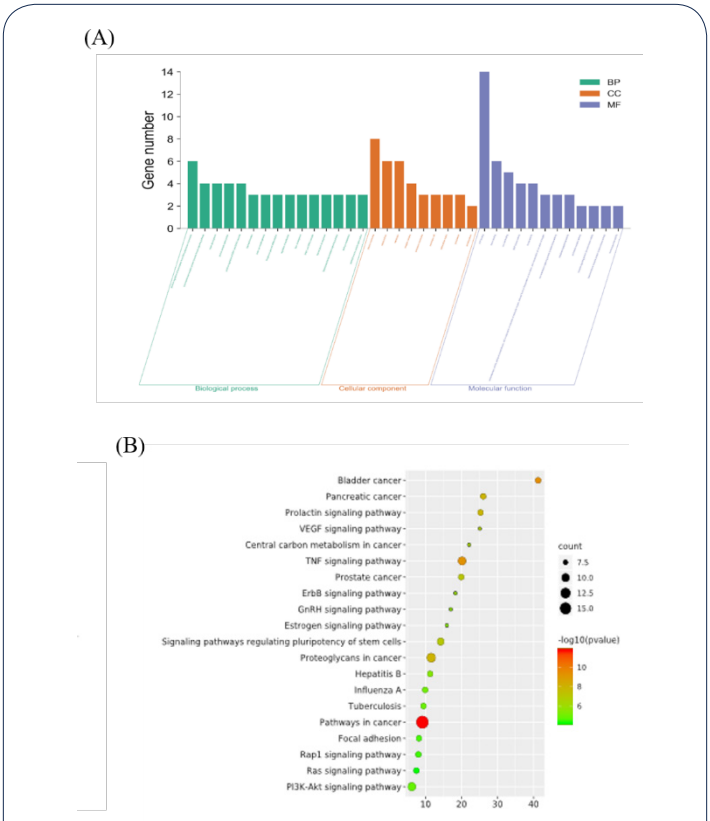

Figure 6: Enrichment analysis. **(A)** GO biological process analysis. **(B)** KEGG pathway enrichment analysis.

Effects of DHA on the proliferation of RKO cells

The equal concentration gradient established in the pre-experiment allowed us to determine the DHA IC_{50} value for RKO cells, which was 94.14 μmol/L. Here, several concentrations (25, 50, and 100 μmol/L) and periods (12, 24, 48, and 72 h) were set based on the IC_{50} value to assess the influence of DHA on the survival of RKO cells by MTT. This allowed us to analyze the anti-CRC activity of DHA. Figure 7 illustrated how increasing the medication dosage and duration of the intervention strengthened the inhibitory impact of DHA on RKO cell growth.

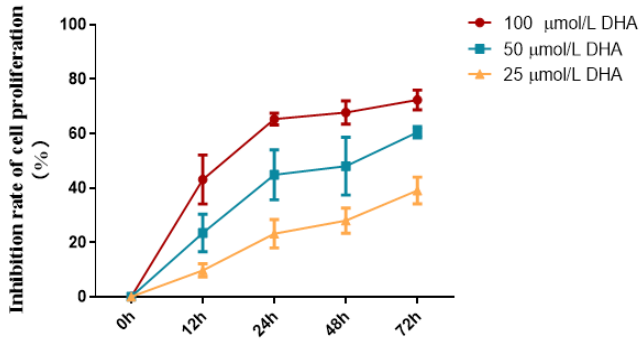

Figure 7: Inhibitory effect of DHA at different concentrations on RKO cell proliferation at different times.

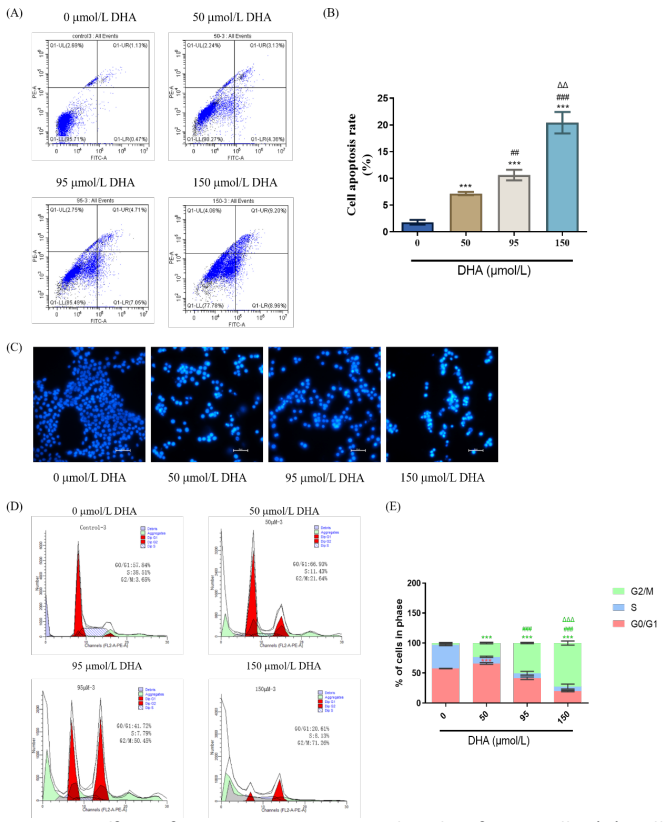

Figure 8: Effect of DHA on apoptosis and cycle of RKO cells. (A) Cell apoptosis was detected by flow cytometry. (B) Cell apoptosis rate in each group (n=3, data represent mean ± SD; ***P*<0.01 vs 0 μmol/L DHA; $^{\#\#}$*P*<0.01 vs 50 μmol/L DHA; $^{\Delta\Delta}$*P*<0.01 vs 95 μmol/L DHA). (C) Hoechst 33258 staining was used to detect cell apoptosis in each group (40×). (D) The cell cycle of RKO in each group was detected by flow cytometry. (E) Effects of different concentrations of DHA on RKO cell cycle (n=3, data represent mean ± SD; ****P*<0.001 vs 0 μmol/L DHA; $^{\#\#\#}$*P*<0.001 vs 50 μmol/L DHA; $^{\Delta\Delta}$*P*<0.001 vs 95 μmol/L DHA).

Effects of DHA on apoptosis and cycle of RKO cells

We investigated how DHA affected the apoptosis of RKO cells using flow cytometry. The effects of different DHA concentrations (50, 95, 150 μmol/L) on the apoptosis of RKO cells were depicted in Figure 8 (A) and (B). The results indicated that, as compared to the 0 μmol/L DHA group, DHA could considerably enhance apoptosis of RKO cells with an increased concentration within 48 h.

With different concentrations of DHA intervention, RKO cells were stained using Hoechst 33258 fluorescent dye. The apoptosis of RKO cells induced by DHA intervention for 48 h was visible under a fluorescent microscope.

As seen in Figure 8(C), the fluorescence intensity gradually deepened as the medication concentration rose, and the number of cells declined. The nucleus ruptured and turned white at a high concentration (150 μmol/L).

The cell cycle alterations in different dosages of DHA treated with PI labeling were discovered using flow cytometry. Figures 8 (D) and (E) demonstrated how DHA damaged RKO cells' DNA and blocked the cell cycle in the G2/M phase, and higher DHA concentrations strengthened the degree of blockage. In Figure 8 (D), it was also noted that the fraction of aggregation (green) and cell debris (blue) increased as DHA concentration rose, indicating an increase in the number of apoptotic cells. It proved that DHA prevented RKO cells from proliferation and inducing apoptosis.

Effects of DHA on the migratory capacity of RKO cells

DHA was tested for its effects on the migration of RKO cells to further confirm its anti-CRC activity. A wound healing experiment was applied to examine the impact of 95 μmol/L DHA intervention at various times (6, 12, and 24 h) on the migratory capacity of RKO cells, as shown in Figures 9 (A) and (B). When compared to the control group (0 μmol/L DHA), DHA had no discernible impact on the RKO cells' capacity for migration at 6 h. However, following 12 and 24 h of treatment, DHA was able to inhibit the survival of RKO cells and dramatically limit their migration (*P*<0.01). Meanwhile, Figure 9 (C) showed that the addition of 95 μmol/L DHA decreased the expression of MMP-9 in RKO cells (*P*<0.05). These results implied that DHA suppressed RKO cell proliferation and migration, which might have the potential application value of the anti-CRC effect.

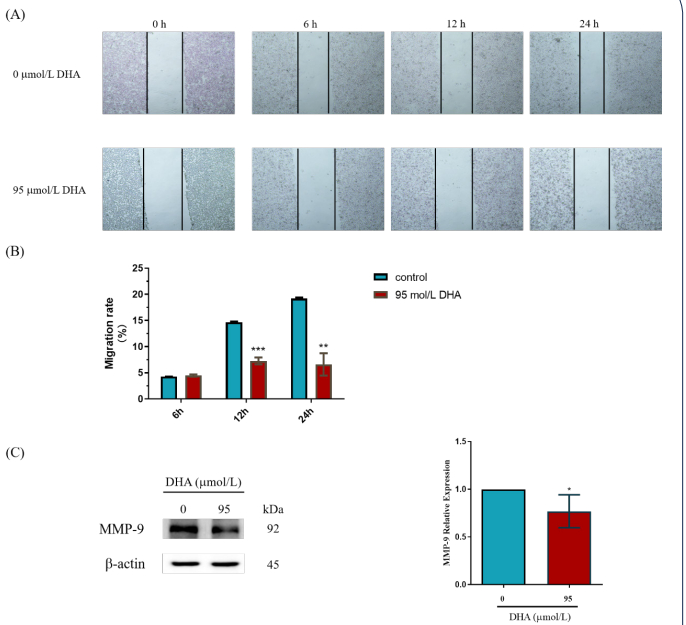

Figure 9: Effect of DHA on the migratory capacity of RKO cells. **(A)** The wound healing test observed cell migration after DHA intervention at different times (4×). **(B)** Cell migration rate in each group (n=3, data represent mean ± SD; ****P*<0.001, ***P*<0.01 vs 0 μmol/L DHA). **(C)** MMP-9 relative expression was detected by Western blotting (n=3, data represent mean ± SD; **P*<0.05 vs 0 μmol/L DHA).

Effects of DHA on mRNA transcript levels of apoptosis-related genes in RKO cells

We detected the activation of the caspase cascade by RT-qPCR and western blot to better comprehend the impact of DHA on RKO cell apoptosis and the molecular mechanism causing apoptosis. The major regulators for endogenous apoptotic pathways are found in mitochondria, which also govern Cyt C release by controlling the Bcl-2 protein family and the permeability of the mitochondrial membrane. To create an "apoptotic body," released Cyt C joins with Apaf-1 and pro-caspase-9. This "apoptotic body" subsequently activates the executive factor caspase-3, resulting in DNA damage and nuclear condensation, which leads to cell apoptosis [18,19]. In RKO cells, RT-qPCR was used to identify the mRNA transcripts of pro-apoptotic factors including *caspase-3*, *caspase-9*, *Bax*, and anti-apoptotic factors like *Bcl-2*, shown in Figure 10 (A). After 12 h of 95 μmol/L DHA intervention, the expression of *caspase-3* and *caspase-9* mRNA in RKO cells was considerably higher than in the control group (0 μmol/L DHA), (P<0.01). The *Bax*/*Bcl-2* mRNA expression ratio was also increased (P<0.05).

Effects of DHA on the expression of apoptosis-related proteins in RKO cells

Figures 10 (B) and (C) indicated the changes in the expression levels of apoptosis-related proteins in RKO cells after DHA intervention. The results demonstrated a considerable up-regulation of cleaved-Caspase-3/Capase-3, cleaved-Caspase-9/Capase-9, and Bax/Bcl-2 protein expression ratios in RKO cells following 48 h intervention with 50 and 95 μmol/L DHA. And compared to the 50 μmol/L DHA, 95 μmol/L DHA showed a more pronounced rise in the expression of apoptosis-related proteins. These results suggested that DHA treatment of RKO cells could induce apoptosis and prevent cell growth by activating the endogenous apoptotic pathway.

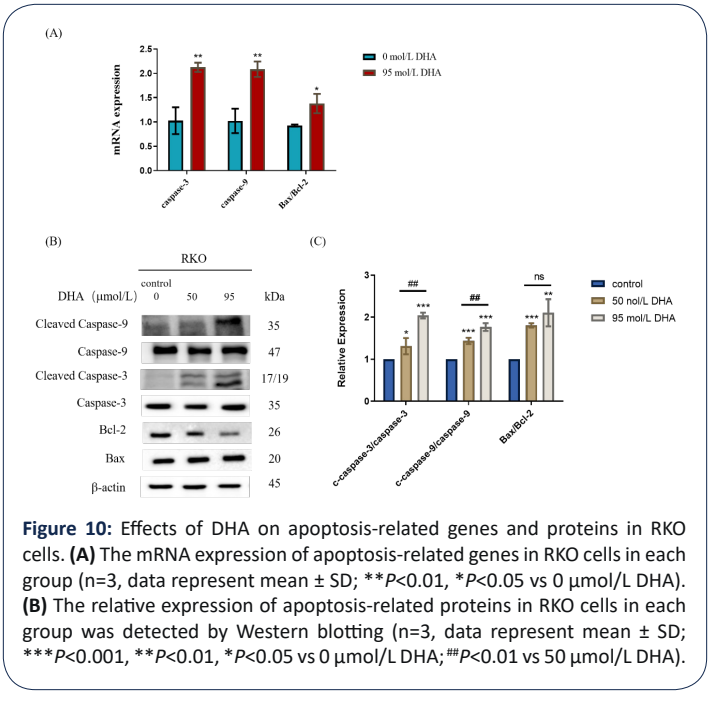

Figure 10: Effects of DHA on apoptosis-related genes and proteins in RKO cells. **(A)** The mRNA expression of apoptosis-related genes in RKO cells in each group (n=3, data represent mean ± SD; **P<0.01, *P<0.05 vs 0 μmol/L DHA). **(B)** The relative expression of apoptosis-related proteins in RKO cells in each group was detected by Western blotting (n=3, data represent mean ± SD; ***P<0.001, **P<0.01, *P<0.05 vs 0 μmol/L DHA; $^{\#\#}P$<0.01 vs 50 μmol/L DHA).

Effects of DHA on the phosphorylation of PI3K, AKT, and p38 MAPK in RKO cells

To support the underlying anti-CRC action of DHA that was discovered utilizing network pharmacology, the expression of proteins linked to the PI3K/AKT pathway was investigated. Western blot was used to analyze the endogenous role of PI3K, AKT, and p38 MAPK in the DHA intervention of RKO cells. As seen in Figure 11, 95 μmol/L DHA significantly reduced the protein expression of AKT and prevented the phosphorylation of p38 MAPK, PI3K, and AKT within 48 h when compared to the control group (0 μmol/L DHA) (P<0.05, P<0.01). These results revealed a connection between DHA's proapoptotic and proliferation-inhibiting effects on RKO cells and the PI3K/AKT signal transduction pathway.

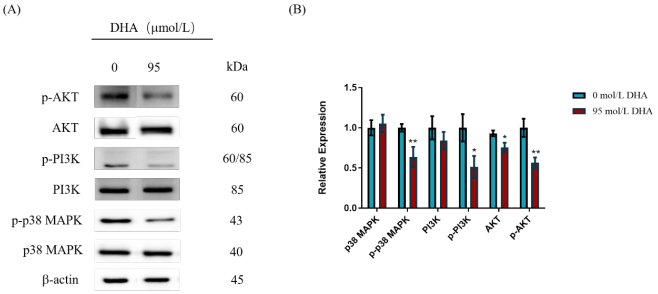

Figure 11: The relative expression of PI3K/AKT signaling pathway-related proteins in RKO cells of each group was detected by Western blotting (n=3, data represent mean ± SD; **P<0.01, *P<0.05 vs 0 μmol/L DHA).

Discussion

The function and molecular mechanism of DHA in the treatment of CRC were investigated in this study using RKO cell lines, and the suppressive impact of DHA on subcutaneous transplanted tumors was evaluated using nude mice. The findings showed that DHA could cause RKO cell apoptosis and decrease tumor growth while not negatively affecting normal cells via blocking p38 MAPK phosphorylation and modifying the PI3K/AKT signaling pathway [20], indicating that DHA is a promising anticancer therapy.

To create the RKO CRC model so that researchers can examine how different DHA concentrations affect CRC xenografts in nude mice. The level of TNF-α expression in the serums of each group after administration was found and examined. The weight of the solid tumor was markedly smaller in the high-dose group than in the model group and the low-dose group, suggesting that a tumor may be suppressed by a high dose of 200 mg/kg DHA. The tumor inhibition rate was 41.45%, whereas the corresponding percentage in the cisplatin group was 60.80%. Additionally, the body weight and subcutaneous tumor volume changes in the mice before and after treatment revealed that while the cisplatin group and the high-dose DHA group significantly inhibited the growth of the transplanted tumor, the cisplatin group decreased the mice's body weight and growth status.

On the other hand, inflammation and the immune system considerably impact the occurrence and growth of tumors. In distinct cellular microenvironments, TNF-α triggers a variety of reactions, including the activation of apoptosis, necrosis, angiogenesis, cell migration, and differentiation. The NF-κB signaling pathway is triggered when TNF-α interacts with the receptor TNF-α, and NF-κB transcription factors cause the expression of

apoptosis inhibitory factors, inhibiting the activation of caspases and preventing tumor cell apoptosis, which promotes tumor growth, invasion, and metastasis [21]. Clinical research findings also revealed that blood samples from CRC patients had much higher levels of TNF-α than samples from healthy individuals [22]. Elisa was used to measure the amount of TNF-α in each group of mice's peripheral blood. Both the high- and low-dose DHA groups dramatically decreased the amount of TNF-α, it was discovered. In comparison to the cisplatin group, the inhibitory effect on the level of TNF-α was more substantial (P<0.05).

The regulation of transcription, translation, proliferation, growth, and survival, as well as other fundamental cell biological processes, is governed by the PI3K/AKT and MAPK signaling pathways. These pathways have a key role in maintaining protein synthesis, fostering proliferation, and preventing apoptosis. Consequently, inappropriate activation of this pathway can result in the emergence and growth of malignancies [23,24]. PI3K is a specific catalyst for phosphatidylinositol, primarily consisting of its regulatory subunit P85 and its catalytic subunit P110. It can be classified into subunits I, II, and III based on the catalytic subunit P110 and its related substrates. According to studies, phosphatidylinositol PIP2 activates the plasma membrane's PI3K diphosphate function. This causes PIP2 to be transformed into PIP3, which is subsequently transferred as a second messenger bound to AKT [25].

The top 5 key targets that are strongly related to DHA in the treatment of CRC were identified by the analysis of PPI Network data by Cytoscape, and molecular docking was carried out to estimate the interaction between receptor and ligand. These findings imply that DHA may inhibit the development of CRC via regulating MAPK3, MAPK1, ERBB2, EGFR, and PIK3CA. PIK3CA participates in the PI3K/AKT signaling pathway and encodes the p110α protein, which is one of the PI3K enzyme's protein subunits. According to studies, when PIK3CA co-mutates with other genes, the PI3K enzyme is continually activated, which results in the development of tumors even though PIK3CA itself does not cause cancers [26]. The ERBB2 gene is also known as the HER2 gene. Numerous malignancies, including ovarian, bladder, and breast cancer, have been linked to the overexpression of the ERBB2 gene, according to studies [27-29]. ERBB2 can regulate the PI3K/AKT signaling pathway, which can impact the multiplication and invasion of tumor cells. The PI3K/AKT signaling route predominantly boosts Ras proteins by dimerization, initiating the phosphorylation cascade. Like ERBB2, EGFR is a key upstream of this signaling pathway [30].

Akt is a part of a signaling complex that also comprises p38 MAPK, MK2, and Hsp27. In human neutrophils, p38 MAPK-dependent MK2 activation functions as PDK2, which can control Akt activity and is crucial for Akt phosphorylation [31]. The phosphorylation of PDK1, PDK2, and its associated gene sites leads to the activation of AKT, which then controls cell division, death, and proliferation. Through a series of anti-apoptotic effects, activated Akt can activate the phosphorylation of Bcl-2, caspase, and FOXOs, ultimately boosting the survival of cancer cells [32,33].

The results showed that 95 μmol/L DHA completely reduced the expression of the AKT protein in RKO cells and significantly suppressed the phosphorylation of p38 MAPK, PI3K, and AKT, while also increasing the levels of caspase-3, caspase-9, and Bax/Bcl-2 in RKO cells, thereby triggering the endogenous apoptosis pathway. RKO cells' motility and viability may both be considerably hampered by DHA (P<0.01). Further evidence that DHA therapy decreased the expression of MMP-9 protein in RKO cells came from a western blot analysis (P<0.05). MMP-9 has been shown to promote angiogenesis and the destruction of the ECM and basement membrane in cancer cells [34]. Reducing MMP-9's activity in the PI3K/AKT pathway can boost the expression of downstream apoptosis-related proteins because MMP-9 is a prominent molecule downstream of the process [35]. These findings indicated that the link between DHA inhibition of RKO cell proliferation and migration as well as apoptosis induction depended on the activities of p38 MAPK, PI3K, and AKT.

Funding: This work was supported by grants from the National Nature Science Foundation of China (No.82003641), the National Science and Technology Major Project (2019ZX09201004-002), and the Shanghai Education Commission budget project (18LK019).

References

1. Yang Q, Hou C, Huang D, Zhuang C, Jiang W, et al. miR-455-5p functions as a potential oncogene by targeting galectin-9 in colon cancer. Oncology letters. 2017; 13: 1958-1964.
2. Li Y, Wu Y, Xia Q, Zhao Y, Zhao R, et al. Platycodon grandiflorus enhances the effect of DDP against lung cancer by down regulating PI3K/Akt signaling pathway. Biomedicine & pharmacotherapy = Biomedecine & pharmacotherapie. 2019; 120: 109496.
3. Han JM, Song HY, Kim KI, Park WY, Park SH, et al. Polysaccharides from Annona muricata leaves protect against cisplatin-induced cytotoxicity in macrophages by alleviating mitochondrial dysfunction. Molecular medicine reports. 2023; 27.
4. Li S, Zhang B. Traditional Chinese medicine network pharmacology: theory, methodology and application. Chinese journal of natural medicines. 2013; 11: 110-120.
5. Hao da C, Xiao PG. Network pharmacology: a Rosetta Stone for traditional Chinese medicine. Drug development research. 2014; 75: 299-312.
6. Tong Y, Liu Y, Zheng H, Zheng L, Liu W, et al. Artemisinin and its derivatives can significantly inhibit lung tumorigenesis and tumor metastasis through Wnt/β-catenin signaling. Oncotarget. 2016; 7: 31413-31428.
7. Wang Z, Li M, Liu Y, Qiao Z, Bai T, et al. Dihydroartemisinin triggers ferroptosis in primary liver cancer cells by promoting and unfolded protein response-induced upregulation of CHAC1 expression. Oncology reports. 2021; 46.
8. Ma Y, Zhang P, Zhang Q, Wang X, Miao Q, et al. Erratum: Dihydroartemisinin suppresses proliferation, migration, the Wnt/β-catenin pathway and EMT via TNKS in gastric cancer. Oncology letters. 2022; 23: 34.
9. Cui W, Fang T, Duan Z, Xiang D, Wang Y, et al. Dihydroartemisinin Sensitizes Esophageal Squamous Cell Carcinoma to Cisplatin by Inhibiting Sonic Hedgehog Signaling. Frontiers in cell and developmental biology. 2020; 8: 596788.
10. Yuan B, Liao F, Shi ZZ, Ren Y, Deng XL, et al. Dihydroartemisinin Inhibits the Proliferation, Colony Formation and Induces Ferroptosis of Lung Cancer Cells by Inhibiting PRIM2/SLC7A11 Axis. OncoTargets and therapy. 2020; 13: 10829-10840.

11. Zhang T, Hu Y, Wang T, Cai P. Dihydroartemisinin inhibits the viability of cervical cancer cells by upregulating caveolin 1 and mitochondrial carrier homolog 2: Involvement of p53 activation and NAD(P)H:quinone oxidoreductase 1 downregulation. International journal of molecular medicine. 2017; 40: 21-30.

12. Kim S, Thiessen PA, Bolton EE, Chen J, Fu G, et al. PubChem Substance and Compound databases. Nucleic acids research. 2016; 44: D1202-13.

13. Gfeller D, Grosdidier A, Wirth M, Daina A, Michielin O, et al. SwissTargetPrediction: a web server for target prediction of bioactive small molecules. Nucleic acids research. 2014; 42(Web Server issue): W32-8.

14. Wu Y, Zhang F, Yang K, Fang S, Bu D, et al. SymMap: an integrative database of traditional Chinese medicine enhanced by symptom mapping. Nucleic acids research. 2019; 47: D1110-d7.

15. Safran M, Chalifa-Caspi V, Shmueli O, Olender T, Lapidot M, et al. Human Gene-Centric Databases at the Weizmann Institute of Science: GeneCards, UDB, CroW 21 and HORDE. Nucleic acids research. 2003; 31: 142-146.

16. von Mering C, Huynen M, Jaeggi D, Schmidt S, Bork P, Snel B. STRING: a database of predicted functional associations between proteins. Nucleic acids research. 2003; 31: 258-261.

17. Huang DW, Sherman BT, Tan Q, Kir J, Liu D, et al. DAVID Bioinformatics Resources: expanded annotation database and novel algorithms to better extract biology from large gene lists. Nucleic acids research. 2007; 35: W169-75.

18. Yang Y, Yu Y, Wang J, Li Y, Li Y, et al. Silica nanoparticles induced intrinsic apoptosis in neuroblastoma SH-SY5Y cells via CytC/Apaf-1 pathway. Environmental toxicology and pharmacology. 2017; 52: 161-169.

19. Lu WN, Zheng FP, Lai DW, Li H. Xuezhikang () reduced renal cell apoptosis in streptozocin-induced diabetic rats through regulation of Bcl-2 family. Chinese journal of integrative medicine. 2016; 22: 611-618.

20. Chen T, Li M, Zhang R, Wang H. Dihydroartemisinin induces apoptosis and sensitizes human ovarian cancer cells to carboplatin therapy. Journal of cellular and molecular medicine. 2009; 13: 1358-1370.

21. Baud V, Karin M. Is NF-kappaB a good target for cancer therapy? Hopes and pitfalls. Nature reviews Drug discovery. 2009; 8: 33-40.

22. Rasool M, Malik A, Waquar S, Ain QT, Rasool R, Asif M, et al. Assessment of clinical variables as predictive markers in the development and progression of colorectal cancer. Bioengineered. 2021; 12: 2288-2298.

23. McCubrey JA, Steelman LS, Chappell WH, Abrams SL, Montalto G, et al. Mutations and deregulation of Ras/Raf/MEK/ERK and PI3K/PTEN/Akt/mTOR cascades which alter therapy response. Oncotarget. 2012; 3: 954-987.

24. Asati V, Mahapatra DK, Bharti SK. PI3K/Akt/mTOR and Ras/Raf/MEK/ERK signaling pathways inhibitors as anticancer agents: Structural and pharmacological perspectives. European journal of medicinal chemistry. 2016; 109: 314-341.

25. Hennessy BT, Smith DL, Ram PT, Lu Y, Mills GB. Exploiting the PI3K/AKT pathway for cancer drug discovery. Nature reviews Drug discovery. 2005; 4: 988-1004.

26. Xu JM, Wang Y, Wang YL, Wang Y, Liu T, et al. PIK3CA Mutations Contribute to Acquired Cetuximab Resistance in Patients with Metastatic Colorectal Cancer. Clinical cancer research : an official journal of the American Association for Cancer Research. 2017; 23: 4602-4616.

27. Ross JS, Gay LM, Wang K, Ali SM, Chumsri S, et al. Nonamplification ERBB2 genomic alterations in 5605 cases of recurrent and metastatic breast cancer: An emerging opportunity for anti-HER2 targeted therapies. Cancer. 2016; 122: 2654-2662.

28. Skrypek N, Vasseur R, Vincent A, Duchêne B, Van Seuningen I, et al. The oncogenic receptor ErbB2 modulates gemcitabine and irinotecan/SN-38 chemoresistance of human pancreatic cancer cells via hCNT1 transporter and multidrug-resistance associated protein MRP-2. Oncotarget. 2015; 6: 10853-10867.

29. Yoshida K, Tsuda M, Matsumoto R, Semba S, Wang L, et al. Exosomes containing ErbB2/CRK induce vascular growth in premetastatic niches and promote metastasis of bladder cancer. Cancer science. 2019; 110: 2119-2132.

30. Kebenko M, Drenckhan A, Gros SJ, Jücker M, Grabinski N, et al. ErbB2 signaling activates the Hedgehog pathway via PI3K-Akt in human esophageal adenocarcinoma: identification of novel targets for concerted therapy concepts. Cellular signalling. 2015; 27: 373-381.

31. Rane MJ, Coxon PY, Powell DW, Webster R, Klein JB, et al. p38 Kinase-dependent MAPKAPK-2 activation functions as 3-phosphoinositide-dependent kinase-2 for Akt in human neutrophils. The Journal of biological chemistry. 2001; 276: 3517-3523.

32. Porta C, Paglino C, Mosca A. Targeting PI3K/Akt/mTOR Signaling in Cancer. Frontiers in oncology. 2014; 4: 64.

33. Huang WC, Hung MC. Induction of Akt activity by chemotherapy confers acquired resistance. Journal of the Formosan Medical Association = Taiwan yi zhi. 2009; 108: 180-194.

34. Lin W, Xie J, Xu N, Huang L, Xu A, et al. Glaucocalyxin A induces G2/M cell cycle arrest and apoptosis through the PI3K/Akt pathway in human bladder cancer cells. International journal of biological sciences. 2018; 14: 418-426.

35. Li C, Qin Y, Zhong Y, Qin Y, Wei Y, et al. Fentanyl inhibits the progression of gastric cancer through the suppression of MMP-9 via the PI3K/Akt signaling pathway. Annals of translational medicine. 2020; 8: 118.